Mansoura Engineering Journal

Volume 49 | Issue 4 Article 19

2024

Design and construction of a novel reciprocating pin-on-plate wear testing machine

Yasser S. Mohamed
Department of Mechanical Engineering, Faculty of Engineering, Alexandria University, Alexandria, Egypt, yasser.saad@alexu.edu.eg

Ahmed Abdelbary
Egyptian Armed Forces, Egypt

ORIGINAL STUDY

Design and Construction of a Novel Reciprocating Pin-on-plate Wear Testing Machine

Yasser S. Mohamed [a,*], Ahmed Abdelbary [b]

[a] Department of Mechanical Engineering, Faculty of Engineering, Alexandria University, Alexandria, Egypt
[b] Egyptian Armed Forces, Egypt

Abstract

This manuscript introduces a new pin-on-plate tribometer established for a study of the tribological behavior of materials at a constant sliding speed. The originality of this test rig lies in its capability to perform six independent tests at the same time. Wear tests can be conducted with high reliability and low error thanks to the high rigidity of the machine. The reciprocating motion of the counterface was designed to be in an arc path. The tribometer has the facility of changing the applied load and the length of the wear path. The test machine can be used to perform both dry and lubricated wear tests at room temperature. Besides, the design allows to measure the sliding temperature of the test samples at contact with the counterface. The current study also reports the results of the first set of experiments. The test rig was used to evaluate the impact of counterface roughness on the wear rate of polytetrafluoroethylene in dry sliding conditions. The obtained results demonstrated that within the range of roughness (Ra = 0.05−0.5 μm), the roughness of the metallic countersurface did not appear to play a significant role in the wear of the tested polymer.

Keywords: Polytetrafluoroethylene, Surface roughness, Tribometer, Wear

1. Introduction

Tribology, by definition, is the study of friction, wear, and lubrication of interacting moving surfaces. In many tribological systems, probably the most important undesired process involves wear, which is frequently produced at rubbing surfaces and is considered the main reason for failure of machine parts. Furthermore, wear is strongly paired with other contributors such as friction, the media, and the type of motion. This is the reason why tribologists focus on increasing the dependability on laboratory experimental tests as a time and cost-effective technique to consider and evaluate the proposed materials or method.

Tribometer is a laboratory device that enable the examination of friction and wear behavior of materials in selective and controlled operating conditions (Abdelbary et al., 2023a). In 1976, the Society of Tribologists and Lubrication Engineers reported that there are more than 240 recognized designs of setups (Benzing, 1976). A careful choice of tribometers can pretend all the serious features of friction or wear issues without the problems associated with the experimentation on real equipment. Contrariwise, a poorly designed wear testing machine can provide entirely inaccurate results (Stachowiak et al., 2004). It is crucial to design a tribometer that can accurately simulate the real system behavior. The tribometer design should also ensure adequate mechanical rigidity to avoid vibration when there is a rapidly varying friction force as well as to allow accurate measurement of wear. Accordingly, many research groups attempted to develop dedicated tribometers to explore contacts occurring at anticipated conditions: speed, load, temperature, or others (Abdelbary et al., 2004; Leveille et al., 2021; Sajewicz and Kulesza, 2007; Zhang et al., 2021; Berglund et al., 2021; Chen et al., 2019; Mohan et al., 2009; BDA et al., 2022).

Received 24 January 2024; revised 30 April 2024; accepted 31 May 2024.
Available online 9 July 2024

* Corresponding author at: 22 Othman Galal Street, Elbaraka Tower No. 1, Moharem Bek, Alexandria, Egypt.
E-mail addresses: yasser.saad@alexu.edu.eg, ym107@yahoo.com (Y.S. Mohamed).

https://doi.org/10.58491/2735-4202.3221

The international standard test method ASTM G99 (International A. ASTM Standard G99, 2004) and ASTM G133 (International A. ASTM Standard G133, 2005) define the general characteristics of sliding wear tests. Yet, the exact values for the operational parameters such as the forms of wear paths and the applied load are not specified in the standards. Thus, researchers can tailor those parameters to simulate the wear modes in real applications. The wear testing apparatuses accommodate test specimens with diverse geometric shapes (e.g., plates, pins, and blocks) and perform different sliding paths (such as unidirectional, reciprocating, spiral, and others).

The common test rig used for studying reciprocating sliding is the pin-on-plate tribometer, which was first introduced in 1950 by Bowden-Leben and has been applied in several researches (Bowden and Tabor, 1950). The friction and wear data obtained from the Bowden-Leben tribometer are often related to the initial stages of wear because the pin makes fewer traverses over the slab in a specific time. The reciprocating motion can be achieved either by a moving pin on a stationary plate or a stationary pin on a moving plate. Still, in both cases, the motion is usually linear and the wear track is a straight line. Also, the changes in the sliding direction in the reciprocating motion occur at each stroke which needs acceleration and deceleration motion correspondingly. According to the used rigs and drive mechanism, the specific sliding velocity profile may differ.

To the best of our knowledge, Sir John Charnley et al. introduced one of the pioneer studies to evaluate the wear of total replacement hip joints in the human body using a pin-on-disk tribometer (Atkinson et al., 1976). His work was followed by hundreds of researchers aimed at investigating the tribological characterization of artificial joints using the traditional pin-on-disk tribometer (D′ et al., 2021; Atkinson et al., 1985; Fisher and Dowson, 1991; Cooper et al., 1993; Fisher, 1994). However, other researchers conducted their investigations using reciprocating pin-on-plate tribometers (Abdelbary et al., 2004; Dowson et al., 1985). It was postulated that the motion profile did not show a noticeable effect on the rate of wear, with the value of wear rate being greater on a reciprocating pin-on-plate test rig in comparison to a unidirectional pin-on-disk tribometer (Fisher and Dowson, 1991).

Experimentally, it was detected that the results measured by unidirectional pin-on-disk tribometers were about two orders of magnitude lower than that obtained from retrieved acetabular cups from ball-and-socket prostheses (Saikko and Calonius, 2003; Dalli et al., 2023). These test results were described by the phenomenon of friction-induced molecular orientation, which is highly related to the sliding direction. In hip joints, the reciprocating sliding path is not in a straight line but takes the form of an arc path, which may affect the experimental results. Therefore, many studies have been conducted to introduce and develop a tribometer that can simulate the type of sliding in the hip joint to obtain accurate results (Towijaya et al., 2017; Choudhury et al., 2014). Another goal of these studies was to rank tribo-materials that is free from uncontrolled implant design effects on the basis of their relative friction and wear characteristics (Baykal et al., 2014). However, works have been performed on joint simulators, in which real prostheses are tested in a laboratory environment that pretends the real physiological conditions (Affatato et al., 2006; Gonzá et al., 2009; Saikko, 2023).

In polymer–metal bearing applications, it is well established that friction resistance and wear mechanism of polymers are governed by the roughness of the counterpart (Abdelbary et al., 2023b; Nunez and Polycarpou, 2015). Reviewing the literature, it was believed that the smoother the counterface, the lower the wear rate. Yet, earlier studies of polymer–metal tribosystems evidenced that there is an optimum value of surface finish that gives a minimum wear rate of the rubbing polymers (Dowson et al., 1985). However, works conducted to study the wear performance of polymer composites advocated that the roughness of the metal counterface did not seem to play any significant role (Blanchet et al., 2010; Lin et al., 2023).

The formation of a transfer film on the metal counterface has a great consequence on the wear resistance of polymers. Polytetrafluoroethylene (PTFE) is one of the polymers that are often known to build a transfer film against a metal counterface. Although there are plenty of studies (Franklin and de Kraker, 2003; Aksulu and Palabiyik, 2008) conducted to investigate the effect of counterface surface roughness on the wear and transfer behavior of PTFE, this topic is still unclear.

The novelty of the present tribometer lies in its capability to conduct six wear tests simultaneously at selected conditions (applied load, dry, or lubricated) for each test with high reliability and low error. The new rig consists of stationary test samples against a reciprocating counter surface in an arc path under load and recording the parameters of interest. With this test rig, it will be possible to measure friction, wear, and temperature along the test duration. The primary aim of this simplified

pin-on-plate tester is to provide a correct rank of tribo-materials concerning their wear resistance at selected test conditions. This new test rig will be used in the present study to investigate the effect of counterface roughness on the wear behavior of PTFE.

2. Design and fabrication of the tribometer

The six-station tribometer is designed to be able to provide a reciprocating motion, in an arc path, to counterface disks. Contact loads are applied by compression springs. The specifications of the tribometer given in Table 1 is chosen to cover the target range of operating conditions.

Fig. 1 represents (a) a photo and (b) a general overview of the test rig, which has a heavy frame to ensure high rigidity, and dynamic stability, and to minimize vibration effects. The device consists of three cast iron plates (1, 10, and 11), two high-density polyethylene (HDPE) plates (2 and 9), a counterface assembly (3), a single-phase induction motor (4), a proximity sensor (5), a gearbox (6), thermocouples (7), a control box (8), and load mechanisms (12). Each component plays a crucial role in the overall functionality of the machine, and their design and placement within the system are carefully considered.

Table 1. Tribometer operating condition specifications.

Sample size (mm)	
Diameter	5–20
Length	10
Working temperature (°C)	Room ambient temperature (≈25)
Sliding speed (mm/s)	35–90
Reciprocating frequency (Hz)	75
Applied load (kg)	1–90 (for each station)
Stroke length (mm)	14–36
Tribometer dimensions (m)	0.5 × 0.5 × 0.7
Power	220V-AC
Tribometer gross weight (kg)	110
Counterface plate dimensions (mm)	
Diameter	40
Thickness	10

The cast iron plates were a crucial component of the machine design. The upper and lower plates have an outer diameter of 320 mm and a thickness of 36 mm. The upper plate has 12 circular holes of diameter 20 mm, with 6 holes used for fixation purposes and the others to minimize the weight of the plate. In addition, six rectangular holes on the upper plate were used for inserting the load mechanisms. The lower plate, however, had all 12 circular holes used for fixation purposes. The middle plate played a different role, serving a specific purpose. It had an outer diameter of 230 mm and a thickness of 27 mm, and its primary function was to hold the counterface assembly. The middle plate was carefully engineered to be placed on a 51126-thrust bearing, which facilitated the rotating motion (in the Yaw direction) from the motor.

The two HDPE plates have an outer diameter of 340 mm and a thickness of 45 mm. Both plates have 12 holes of 20 mm diameter, with six holes used for fixation purposes and the other six used to minimize mass. In addition, the upper plate had six holes of 43 mm diameter, which are specifically designed to support the load mechanisms. The eight cylinders are placed between the plates to provide support and fix the distances between them.

2.1. Loading mechanism

The loading mechanism is carefully designed and engineered to perform its function effectively and to

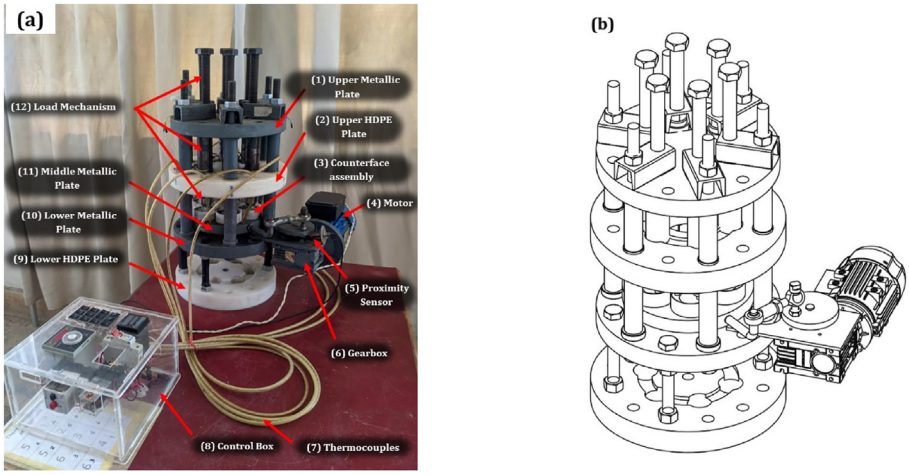

Fig. 1. (a) Photo and (b) a general overview of the test rig.

deliver accurate results. The wear specimens are held vertically in contact with the metallic counterface, while the loads are designed to be normal to the top of the pin holder. As shown in Fig. 2, the mechanism consists of (1) a specimen holder, (2) a compression spring for transmitting the force from the output linear motion of the bolt, (3) a cylinder for protecting the spring, and (4) a channel bracket. The channel bracket has a nut welded to one side, which allows it to engage with (5) a bolt of a 3 mm pitch thread.

2.2. Counterface assembly and driving mechanism

The counterface assembly consists of six hollow cylinders where the stainless steel counterface disks were fixed. The six stations encouraged us to perform six wear tests at the same time to save time. Thanks to the complete separation of each station from the others, as shown in Fig. 3a, we can perform six wear tests under different experimental conditions (applied load, dry, or lubrication) at the same time. However, up to six identical (under the same experimental conditions) wear experiments can be conducted simultaneously.

The machine's performance is dependent on a 0.25 kW, 1400 rpm single-phase induction motor with a trade name Omeik MY711-4. The motor is coupled with a 1:20 reduction gearbox (NMRV 040-20-71B5) giving an output of 70 rpm. The acquired reciprocating motion is generated by a special mechanism, as shown in Fig. 3. The mechanism consists of a steel disk, (1) which is connected to the gearbox output shaft and an adjustable lever (2) with a ball-and-socket end (3). Through this mechanism, the rotation motion of the gearbox output shaft is transformed into a reciprocating motion of the lower cast iron plate (4) and, therefore, the six counterfaces (5). The stroke (wear path) length can be easily controlled by the adjustable lever. In the present tests, the stroke length is selected to be 24 mm.

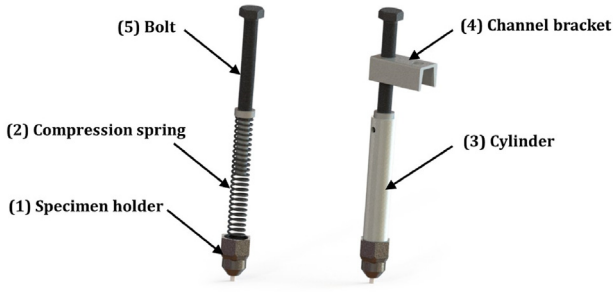

Fig. 2. Loading mechanism.

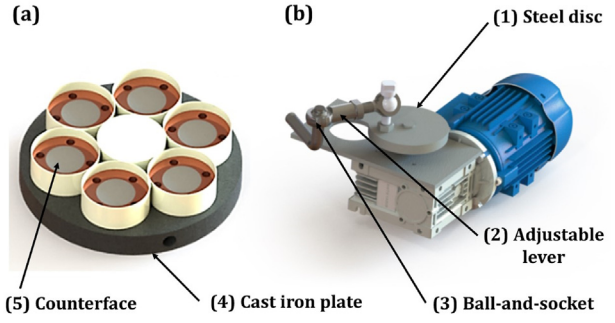

Fig. 3. (a) Counterface assembly and (b) driving mechanism.

2.3. Cast iron and HDPE plates

The upper and lower cast iron plates have an outer diameter of 320 mm and a thickness of 36 mm. The upper plate has 12 circular holes of 20 mm diameter; six are used for fixation purposes and the others to reduce the weight of the plate. An additional six rectangular holes on the upper plate are used for supporting the load mechanisms. The lower plate has 12 circular holes used for fixation purposes. The middle plate has a 230 mm outer diameter and a thickness of 27 mm. The primary function of this plate is to hold the counterface assembly. The middle plate was carefully engineered to sit on a 51126-thrust bearing, which facilitated the rotary motion (yaw) from the driving motor. The two HDPE plates of 340 mm outer diameter and 45 mm thickness are used for fixation and supporting the load mechanisms. Eight cylinders are placed between the plates to provide support and fix the distances between them.

2.4. Sensors and electrical devices

An inductive proximity sensor is a type of sensor commonly used in industrial applications to detect the presence or absence of metallic objects. In this study, an inductive proximity sensor (5), as shown in Fig. 1a, is used as a safety sensor to ensure that the machine operates for a predetermined period and to prevent any potential safety hazards that may arise from prolonged operation. An Autonics counter timer CT6S-1P is used to monitor the number of revolutions detected by the inductive proximity sensor, which promotes tracking the duration of the wear test. The CT6S-1P was configured to count up and display the number of revolutions detected and to trigger a visual and audible alarm when a preset value is reached.

To monitor the temperature of the counterfaces, six thermocouples connected to a temperature control unit are used one for each counterface. The

temperature control unit displays the thermocouple measurements on a digital screen. Furthermore, motor protection switches and circuit breakers are used to protect electric motors from damage due to overloads and electrical faults to ensure a safe operation.

2.5. Stress analysis of tribometer parts

The finite element (FE) analysis shows the behavior of the machine under applied loads, ensuring the minimum deformation with respect to the applied loads. Taking the weight and strength factors into consideration, a stress analysis using the FE method is conducted to determine:

(a) The maximum pressure that the upper plate can withstand.
(b) The maximum deflection that deforms the parts.
(c) The factor of safety of each part.

As demonstrated in all of the FE analyses conducted on the machine parts the factor of safety is found to be significantly high, as shown in Figs. 4–11. The loading and boundary conditions (BC) can be found in the figures where the green and red arrows refer to the fixation and the applied loads, respectively. We optimized the design to ensure that the machine is strong enough to perform its intended functions and has the minimum possible weight. Henceforth, we can achieve a balance between strength and weight, resulting in a more efficient and practical design. The optimization process required careful consideration of various factors such as material selection, structural design, and stress distribution. Table 2 presents the properties of the materials used in FE analysis for the basic parts of the tribometer.

BC: Fixed support on the contact area between the six hollow vertical cylinders under the plate, six loads of 150 N are applied on the six circular areas under the counterface.

Maximum stress = $4.328*10^5$ N/m^2
Minimum safety factor = 715.8
Maximum displacement = $1.009*10^{-4}$ mm

BC: Fixed support on the contact area between the bearing under the plate, six loads of 150 N is applied on the six circular areas under the counterface.

Maximum stress = $8.828*10^5$ N/m^2
Minimum safety factor = 300.8
Maximum displacement = $9.075*10^{-5}$ mm

BC: Fixed support on the contact area between the six hollow vertical cylinders under the plate, on the top of the plate, there is a total force of 100 N applied at the contact area between the gearbox holder and the plate.

Maximum stress = $1.624*10^6$ N/m^2

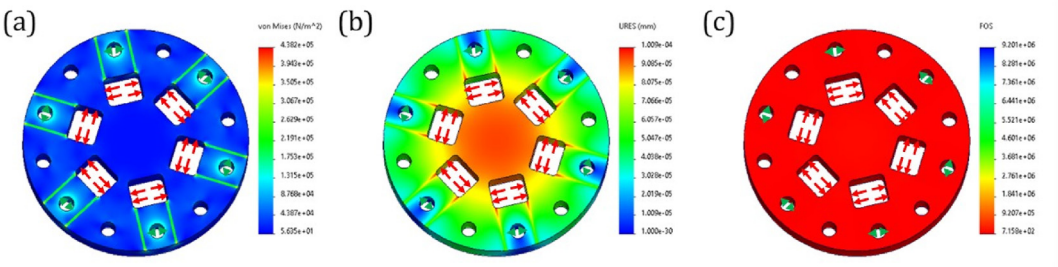

Fig. 4. Finite element analysis results of the upper metallic plate: (a) stress analysis; (b) displacement; and (c) safety factor. BC: Fixed support on the contact area between the 6 hollow vertical cylinders under the plate, six loads 150N is applied on the 6 circular area under the counter face. Maximum stress = $4.328*10^5$ N/m^2. Minimum safety factor = 715.8. Maximum displacement = $1.009*10^{-4}$ mm.

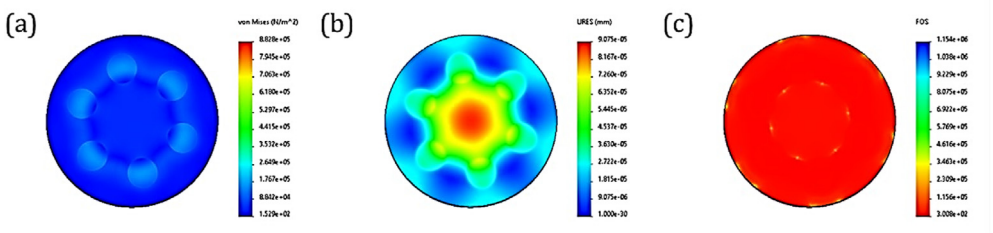

Fig. 5. Finite element analysis results of the middle metallic plate: (a) stress analysis; (b) displacement; and (c) safety factor. BC: Fixed support on the contact area between the bearing under the plate, six loads 150N is applied on the 6 circular area under the counter face. Maximum stress = $8.828*10^5$ N/m^2. Minimum safety factor = 300.8. Maximum displacement = $9.075*10^{-5}$ mm.

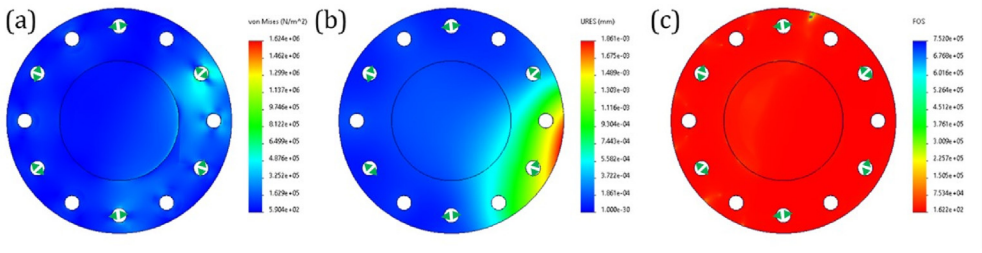

Fig. 6. Finite element analysis results of the lower metallic plate: (a) stress analysis; (b) displacement; and (c) safety factor. BC: Fixed support on the contact area between the 6 hollow vertical cylinders under the plate, on the top of the plate, there is a total force of 100N applied at the contact area between the gearbox holder and the plate. Maximum stress = $1.624*10^{6}$ N/m^2. Minimum safety factor = 162.2. Maximum displacement = $1.861*10^{-3}$ mm.

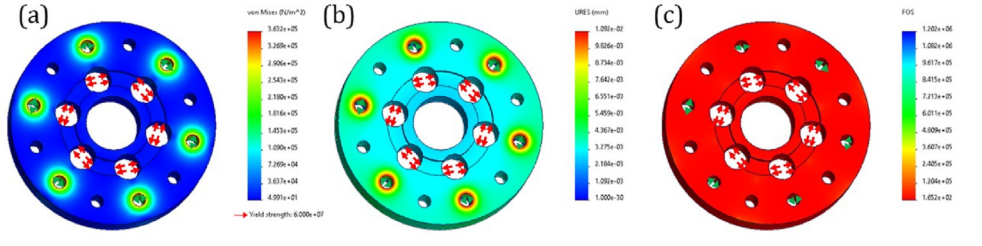

Fig. 7. Finite element analysis results of the upper HDPE plate: (a) stress analysis; (b) displacement; and (c) safety factor. BC: Fixed support on the contact area between the 6 hollow vertical cylinders under the plate, on the contact area between the 6 hollow vertical cylinders above the plate, there is a force was calculated from the upper parts weight. Maximum stress = $3.632*10^{5}$ N/m^2. Minimum safety factor = 165.2. Maximum displacement = $1.092*10^{-2}$ mm.

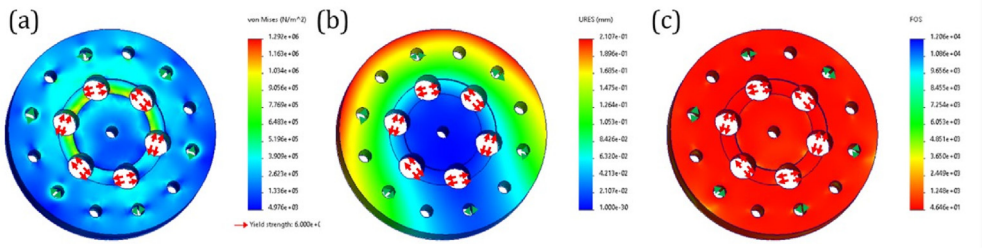

Fig. 8. Finite element analysis results of the lower HDPE plate: (a) stress analysis; (b) displacement; and (c) safety factor. BC: Fixed support on the contact area between the table and the plate, on the contact area between the 5 nuts above the plate, there is a force was calculated from the upper parts weight. Maximum stress = $1.292*10^{6}$ N/m^2. Minimum safety factor = 46.46. Maximum displacement = $2.107*10^{-1}$ mm.

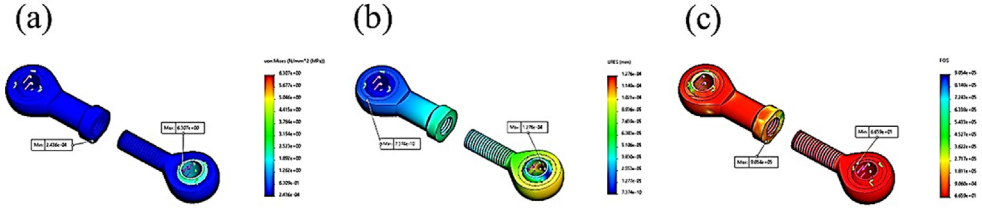

Fig. 9. Fig. 9. Finite element analysis results of the adjustable lever: (a) stress analysis; (b) displacement; and (c) safety factor. Maximum stress = $6.307*10^{6}$ N/m^2. Minimum safety factor = 6.66. Maximum displacement = $1.276*10^{-4}$ mm.

Minimum safety factor = 162.2

Maximum displacement = $1.861*10^{-3}$ mm

BC: Fixed support on the contact area between the six hollow vertical cylinders under the plate; on the contact area between the six hollow vertical cylinders above the plate, there is a force calculated from the weight of the upper parts.

Maximum stress = $3.632*10^{5}$ N/m^2

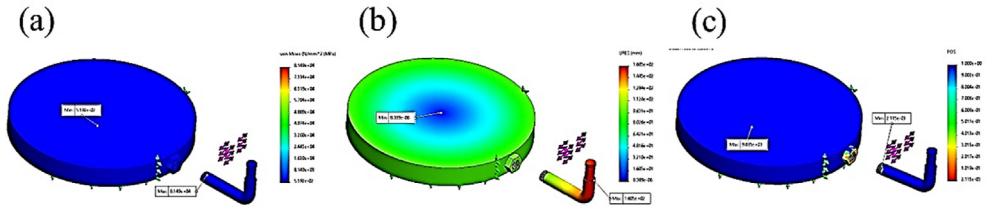

*Fig. 10. Finite element analysis results of the lower cast iron plate with lever: (a) stress analysis; (b) displacement; and (c) safety factor. Maximum stress = 6.307*10^6 N/m^2. Minimum safety factor = 6.66. Maximum displacement = 1.276*10^{-4} mm.*

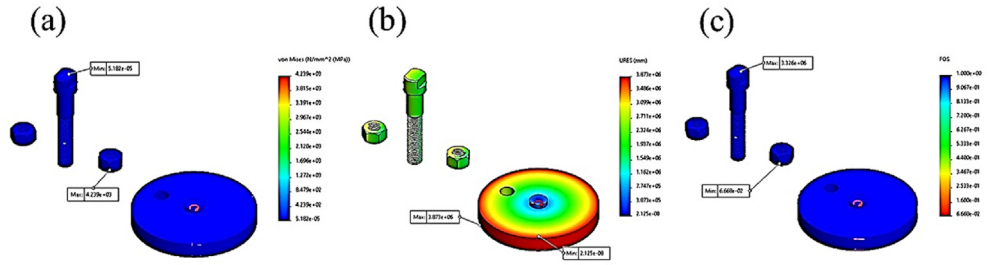

*Fig. 11. Finite element analysis results of the steel disc with bolt: (a) stress analysis; (b) displacement; and (c) safety factor. Maximum stress = 6.307*10^6 N/m^2. Minimum safety factor = 6.66. Maximum displacement = 1.276*10^{-4} mm.*

Table 2. Material properties of the materials used in finite element analysis for three basic components of the tribometer.

Property	Plates Cast iron	Plates HDPE	Adjustable rod Steel (AISI 1020)
Ultimate tensile strength, MPa	151.6	18	420
Tensile yield strength, MPa	–	27	351
Elastic modulus, GPa	66.1	0.6	200
Compressive strength, MPa	572.2	14	–
Mass density, kg/m^3	7200	950	7900

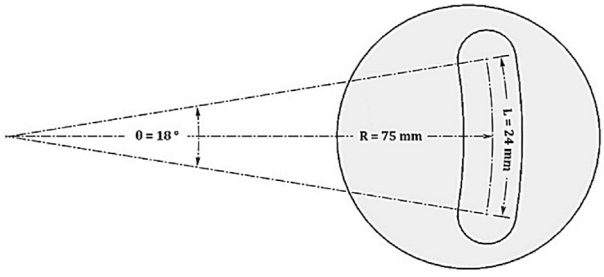

Fig. 12. Wear path.

3. Experimental work

As mentioned above, the principle of operation of the tribometer involves the reciprocating motion of a stationary test specimen against a reciprocating counter surface (disk) in an arc path, as illustrated in Fig. 12. The summary of the wear experiment is indicated in Table 3.

The tribometer is used to evaluate the effect of counterface roughness on the wear behavior of polytetrafluoroethylene (PTFE) polymer.

Stainless steel disks of diameter 40 mm and thickness 12 mm are used as a metallic counterface. The plates were prepared by surface finishing to provide four different surface roughnesses with a centerline average (Ra) as indicated below. All wear tests were performed in a dry sliding condition.

The polymer specimens were carefully cleaned using ethyl alcohol, after that it was dried at 60–70 °C in an oven. Before roughness measurements, the metallic disks were cleaned using petroleum ether and cleaned again using ethyl alcohol just before the wear experiments. Roughness measurements were performed on the cylindrical surface of the disks in axial and

Table 3. Summary of wear experiments.

Parameter	Value
Specimen material	PTFE
Applied load (N)	65
Nominal surface area of the specimen (mm^2)	63.6
Nominal applied pressure (MPa)	1.02
pv factor (MPa.m/s)	0.061
Average sliding speed (m/s)	0.06
Oscillation stroke (mm)	24
Room temperature (°C)	20–25
Relative humidity (%)	30–50
Counterface roughness (Ra) (μm)	0.05, 0.15, 0.25, and 0.5
Total sliding distance (m)	3672
Maximum allowable temperature (°C)	42

circumferential directions, using a MAHR Perthometer Concept stylus instrument with a 2 μm stylus tip radius. The axial measurements were taken using a conventional straight drive unit with a moving probe, but the circumferential measurements were taken using a rotational drive unit while the probe was stable. The cutoff wavelength was 0.25 mm, the evaluation length was 4 mm, and the horizontal resolution of the profiles was 0.7 μm. In every measurement, raw profile data and standard roughness parameters were saved.

All wear tests were conducted under a 65 N normal applied load for a total sliding distance of 3672 m. After setting up the required applied load, tests were run and the counterface temperature was measured every 10 min to ensure it was below the allowable temperature (42 °C). After each run, PTFE specimens were carefully removed and volumetric worn material was calculated. For each roughness value, the wear tests were repeated three times and the mean of wear rate is given in the table of the results. Wear curves were plotted based on experimental results.

4. Results and discussion

Wear rates of PTFE samples tested against different counterface roughnesses are presented in Table 4, while Fig. 13 shows a typical wear graph of dry wear tests with all the points marked, the points fitting very well to the straight lines in wear regimes. The wear curve possesses two regions, the first regime of sliding is the running-in wear followed by steady-state wear. Curve fitting was applied to obtain the wear rates WR at the steady-state wear regime. The wear rates were calculated from

$$WR = \frac{V}{X}\ (\mathrm{mm}^3/\mathrm{m}) \qquad (1)$$

where

V is the worn volume (mm^3) and

X is the sliding distance (m).

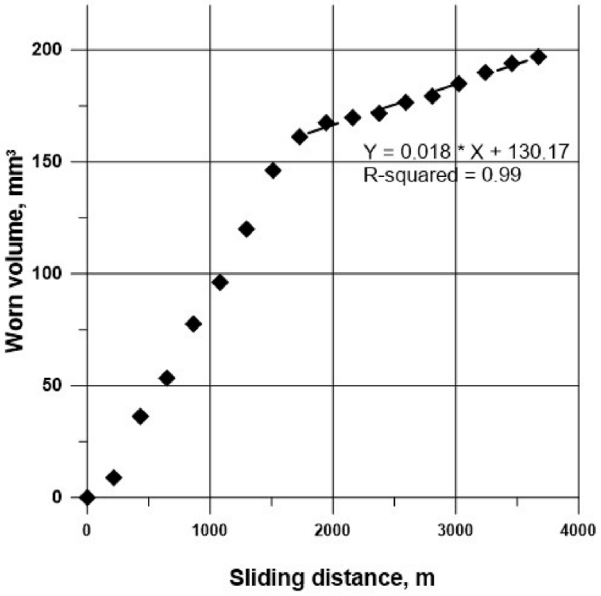

Fig. 13. A typical graph of dry wear tests (Test no. 2).

All tests showed a typical wear curve as shown in Fig. 13. The curve can be divided into two distinct zones: (1) the running-in regime which is related to the removal of the artificial (manufacturing) surface of the PTFE specimen, which is characterized by a relatively higher wear rate and (2) steady-state wear which has a lower and linear wear rate and characterized by the formation of a stable transfer film layer of PTFE polymer, which wears in a steady and uniform way. This observation was widely mentioned and discussed in many past literature (Stachowiak et al., 2006; Abdelbary, 2014). Fig. 14 shows the variation of the steady-state wear rate of PTFE with counterface roughness. The wear rate of PTFE did not show any significant variation with the variation of counterface roughness. This finding is attributed to the wear mechanism of unlubricated polymer–metal sliding, where the wear of a polymer involves abrasion and adhesion mechanisms. The abrasion wear frequently occurs at the first stage of wear (running-in phase) and includes

Table 4. Results of wear test.

Test No.	Counterface roughness Ra, (μm)			Running-in wear		Steady-state wear		
	At the start of the test	At the end	Total volume loss (mm^3)	Average siding temperature[a] (°C)	Wear rate (mm^3/m)[a]10^{-3}	Average siding temperature[a] (°C)	Wear rate, average[b] (mm^3/m)[a]10^{-3}	St. dev. R^2
1	0.05	0.1	140	29	67.2	30	16.7	0.992
2	0.15	0.1	195	28	98.2	28	16.9	0.987
3	0.25	0.1	185	29	80.8	27	17.4	0.953
4	0.5	0.3	160	28	82.1	30	16.8	0.912

[a] Near contact temperature.
[b] Arithmetic means of three test results.

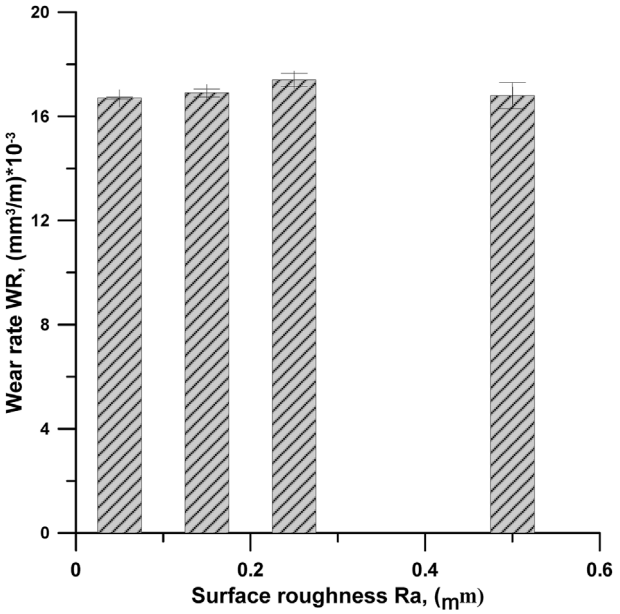

Fig. 14. Variation of wear rate (WR) of PTFE with counterface roughness (Ra).

'debris' particles. Adhesion wear, however, occurs at relatively smoother counterfaces and results in transferred particles (transfer film). The wear rate depends on the combined effect of these two mechanisms. At the first stage (running-in), the wear of the PTFE was due to micro-cutting and plowing of the rough peaks at the metallic counterface, as shown in Fig. 15. The worn PTFE adhered to the stainless-steel counterface and filled the valleys of its surface forming a polymer transfer film layer that protects the specimen's surface from metal asperities and changed the friction interface into polymer–polymer sliding.

As shown in Table 2, although the formation of the transfer film reduced the counterface surface roughness (Ra = 0.15–0.5 μm), at the lowest counterface (Ra = 0.05 μm), the formation of transfer film resulted in increasing the roughness (Ra = 0.1 μm), which is attributed to the mechanism of wear (adhesion) at smooth counterfaces (Abdelbary et al., 2023b). After a certain sliding distance, a steady-state regime is reached at which equilibrium is reached between the polymer transferred to the counterface and that removed from the wear track. One of the interesting consequences of polymer transfer is a change in the topography of both the rubbing surfaces in contact. The roughness of the PTFE specimen's surface undergoes large variation during the running-in wear until the steady-state wear is reached, while the roughness of the steel counterface surface is modified due to the transfer of the polymer. Therefore, the sliding mechanism can be roughly described as a sliding of PTFE on itself, this can be the reason that the values of the wear rate of all tests were very close to each other (about $17*10^{-3}$ mm^3/m), while the variation was less than 5%. The obtained wear rates were comparable to those found in other literature (Lancaster, 1971; Kolhe et al., 2019; Viswanath and Bellow, 1995; Dhanumalayan and Joshi, 2018) under similar experimental conditions.

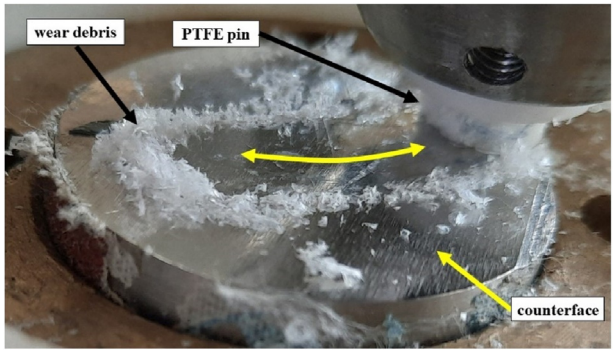

Fig. 15. Wear of PTFE specimen, Test no. 2 after 1000 m sliding distance.

For the selected range of roughness (0.05–0.5 μm), the roughness of the steel countersurface did not seem to play a significant role in the wear behavior of pure PTFE. At a relatively low roughness range (0.05–0.2 μm), tests 1, 2, and 3, the PTFE polymer adhered to the stainless-steel disk surface rather than abrasion, and the wear rate increased with the increase of Ra. However, at higher roughness values within the range 0.5–0.7 μm, tests 3 and 4, WR decreased to reach a minimum value of 82×10^{-3} mm^3/m for Ra = 0.7 μm as shown in Table 2.

5. Conclusion

The current manuscript has presented a new pin-on-plate reciprocating tribometer developed for studying the wear behavior of polymers. The designed six-station tribometer can perform wear tests in dry or lubricated working conditions with high reliability and low error thanks to the high rigidity of the machine. The test rig can be used to evaluate the wear performance of up to six test samples for applied loads of up to 90 kg for each. The wear tests can be performed at varying stroke lengths (from 14 to 36 mm) and a sliding speed range (from 35 to 90 mm/s) at a reciprocating frequency of Hz. PTFE test specimens sliding in dry conditions on stainless steel counterfaces were investigated to explore the effect of counterface surface roughness on the wear behavior using the

new tribometer. Based on the experimental findings we can highlight the following:

(a) Within the range of roughness (Ra = 0.05–0.5 μm), the stainless steel countersurface roughness does not appear to play an important role in the steady-state wear rate of PTFE polymer.
(b) At a steady-state wear regime, the formation of a PTFE transfer film fills the counterface valise and protects the rubbing surface of the PTFE samples from the counterface asperities.

Conflict of interest

There are no conflicts of interest.

Funding

The current study is a self-funding work, with no funders or grants.

Author contribution

It is a collaborative work where Yasser S. Mohamed and Ahmed Abdelbary worked together. Yasser S. Mohamed conceived the idea and designed the testing machine. Ahmed Abdelbary designed the experiments. Both authors performed data analysis, wrote, developed the paper and agreed to the published version of the manuscript.

References

Abdelbary, A., 2014. 2 - sliding mechanics of polymers. In: Abdelbary, A. (Ed.), Wear of Polymers and Composites. Woodhead Publishing, Oxford, United Kingdom, pp. 37–66.
Abdelbary, A., et al., 2004. A new reciprocating tribometer for wear testing under different fluctuating loading conditions. Alex. Eng. J. 43, 615–619. Alexandria, Egypt.
Abdelbary, A., Chang, L., 2023a. 9 - Tribology testing, measurements, and evaluation. In: Abdelbary, A., Chang, L. (Eds.), Principles of Engineering Tribology. Academic Press, United Kingdom, pp. 391–453.
Abdelbary, A., Chang, L., 2023b. 6 - Tribology of nonmetals. In: Abdelbary, A., Chang, L. (Eds.), Principles of Engineering Tribology. Academic Press, United Kingdom, pp. 235–294.
Affatato, S., Leardini, W., Zavalloni, M., 2006. Hip joint simulators: state of the Art. In: Bioceramics and Alternative Bearings in Joint Arthroplasty. Steinkopff, Darmstadt.
Aksulu, M., Palabiyik, M., 2008. Effect of Counterface Roughness on the Wear of Polyoximethylene and Polypropylene, pp. 463–471.
Atkinson, J.R., et al., 1976. The wear of total replacement hip joints in the human body-A topgraphical survey of the surfaces of worn acetabular cups. In: Third Leeds – Lyon Symposium on Tribology.
Atkinson, J.R., et al., 1985. Laboratory wear tests and clinical observations of the penetration of femoral heads into acetabular cups in total replacement hip joints: III: the measurement of internal volume changes in explanted Charnley sockets after 2–16 years in vivo and the determination of. wear factors. Wear 104, 225–244.
Baykal, D., et al., 2014. Advances in tribological testing of artificial joint biomaterials using multidirectional pin-on-disk testers. J. Mech. Behav. Biomed. Mater. 31, 117–134.
BDA, Hidalgo, et al., 2022. Design of pin on disk tribometer under international standards. In: Applications of Computational Methods in Manufacturing and Product Design. Springer Nature Singapore, Singapore.
Benzing, R.J., 1976. Friction and Wear Devices : Revised and Enlarged Report of Subcommittee on Wear, Lubrication Fundamentals Committee. American Society of Lubrication Engineers, Basel, Switzerland.
Berglund, K., et al., 2021. A novel reciprocating tribometer for friction and wear measurements with high contact pressure and large area contact configurations. Lubricants 9 (12), 123. https://doi.org/10.3390/lubricants9120123.
Blanchet, T.A., Kandanur, S.S., Schadler, L.S., 2010. Coupled effect of filler content and countersurface roughness on PTFE nanocomposite wear resistance. Tribol. Lett. 40, 11–21. Switzerland AG.
Bowden, F.P., Tabor, D., 1950. The Friction and Lubrication of Solids. Clarendon Press Oxford, U.K.
Chen, S., et al., 2019. A novel tribometer for investigating bushing wear. Wear 430–431, 263–271.
Choudhury, D., et al., 2014. Tribological investigation of ultra-high molecular weight polyethylene against advanced ceramic surfaces in total hip joint replacement. In: Proceedings of the Institution of Mechanical Engineers, Part J: Journal of Engineering Tribology, vol. 229, pp. 410–419.
Cooper, J.R., Dowson, D., Fisher, J., 1993. Macroscopic and microscopic wear mechanisms in ultra-high molecular weight polyethylene. Wear 162–164, 378–384.
Dalli, D., et al., 2023. Polyethylene wear simulation models applied to a prosthetic hip joint based on unidirectional articulations. J. Mech. Behav. Biomed. Mater. 142, 105882.
Dhanumalayan, E., Joshi, G.M., 2018. Performance properties and applications of polytetrafluoroethylene (PTFE)—a review. Adv. Compos. Hybrid Mater. 1, 247–268.
Dowson, D., et al., 1985. Influence of counterface topography on the wear of ultra high molecular weight polyethylene under wet or dry conditions. In: Polymer Wear and its Control. American Chemical Society, Amsterdam, Netherlands, pp. 171–187.
D'Andrea, D., et al., 2021. Tribological characterization of a hip prosthesis in Si3N4-TiN ceramic composite made with Electrical Discharge Machining (EDM). Procedia Struct. Integr. 33, 469–481.
Fisher, J., 1994. Wear of ultra high molecular weight polyethylene in total artificial joints. Curr. Orthop. 8, 164–169.
Fisher, J., Dowson, D., 1991. Tribology of total artificial joints. Proc. IME H J. Eng. Med. 205, 73–79.
Franklin, S.E., de Kraker, A., 2003. Investigation of counterface surface topography effects on the wear and transfer behaviour of a POM–20% PTFE composite. Wear 255, 766–773.
González-Mora, V.A., et al., 2009. Wear tests in a hip joint simulator of different CoCrMo counterfaces on UHMWPE. Mater. Sci. Eng. C 29, 153–158.
International A. ASTM Standard G133, 2005. Standard Test Method for Linearly Reciprocating Ball-on-Flat Sliding Wear. West Conshohocken, PA.
International A. ASTM Standard G99, 2004. Standard Test Method for Wear Testing with a Pin-On-Disk Apparatus. West Conshohocken, PA.

Kolhe, S., Deshpande, A., Wangikar, K., 2019. Wear behavior of polytetrafluoroethylene composites: a review. In: Smart Technologies for Energy, Environment and Sustainable Development. Springer Singapore, Singapore.

Lancaster, J.K., 1971. Estimation of the limiting PV relationships for thermoplastic bearing materials. Tribology 4, 82−86, 6 figs., 8 refs. Wear, 1972. 19(3):364.

Leveille, T., et al., 2021. Development of a novel high temperature open tribometer with laser-based heating system. Wear 477, 203881. Amsterdam, Netherlands.

Lin, Z., et al., 2023. Coupled effect of filler and countersurface roughness on the tribological performance of the PEEK-PTFE-steel hybrid wear system. Wear 523, 204841.

Mohan, C.B., et al., 2009. Design and development of an advanced linear reciprocating tribometer. Wear 267, 1111−1116.

Nunez, E.E., Polycarpou, A.A., 2015. The effect of surface roughness on the transfer of polymer films under unlubricated testing conditions. Wear 326−327, 74−83.

Saikko, V., 2023. VEXLPE friction studied with a multidirectional hip joint simulator using contact temperature control. Tribol. Int. 187, 108707.

Saikko, V., Calonius, O., 2003. An improved method of computing the wear factor for total hip prostheses involving the variation of relative motion and contact pressure with location on the bearing surface. J. Biomech. 36, 1819−1827.

Sajewicz, E., Kulesza, Z., 2007. A new tribometer for friction and wear studies of dental materials and hard tooth tissues. Tribol. Int. 40, 885−895.

Stachowiak, G.W., Batchelor, A.W., Stachowiak, G.B., 2004. 3 - tribometers. In: Stachowiak, G.W., Batchelor, A.W., Stachowiak, G.B. (Eds.), Tribology Series. Elsevier, pp. 25−78.

Stachowiak, G.W., Batchelor, A.W., 2006. 16 - wear of non-metallic materials. In: Stachowiak, G.W., Batchelor, A.W. (Eds.), Engineering Tribology, third ed. Butterworth-Heinemann, Burlington, pp. 651−704.

Towijaya, T., Ismail, R., Jamari, J., 2017. Design of a hip prosthetic tribometer based on salat gait cycle. AIP Conf. Proc. 1788, 030071.

Viswanath, N., Bellow, D.G., 1995. Development of an equation for the wear of polymers. Wear 181−183, 42−49.

Zhang, T., et al., 2021. A novel ultrahigh-speed ball-on-disc tribometer. Tribol. Int. 157, 106901.